frontiers | Frontiers in Materials

ORIGINAL RESEARCH
published: 08 June 2022
doi: 10.3389/fmats.2022.887864

First-Principles Calculations of the Exchange Interaction of the $CrGeTe_3$/NiO Interface

*Xuehua Liu[1], Zhaoyuan Li[1], Whenli Zhang[1], Pei Yao[1], Haoran Zhu[1], Xin Liu[1] and Xu Zuo[1,2,3]**

[1]College of Electronic Information and Optical Engineering, Nankai University, Tianjin, China, [2]Key Laboratory of Photoelectronic Thin Film Devices and Technology of Tianjin, Nankai University, Tianjin, China, [3]Engineering Research Center of Thin Film Optoelectronics Technology, Ministry of Education, Nankai University, Tianjin, China

Two-dimensional (2D) magnetic materials have recently attracted a great attention due to their potential applications in information processing and storage. It was observed in an experiment that the $CrGeTe_3$/NiO heterostructure shows a higher Curie temperature and a stronger perpendicular anisotropy. This suggests that antiferromagnet NiO can be coupled with ferromagnetic $CrGeTe_3$ by the proximity effect, which enhances ferromagnetism. However, the mechanism behind the coupling is unknown. In this work, we built a $CrGeTe_3$/NiO heterostructure model and investigated the electronic structure and magnetic properties of the $CrGeTe_3$/NiO interface by first-principles calculations. It is shown that the intralayer exchange interaction between the Cr atoms is ferromagnetic, and the interlayer exchange interaction between the Ni atoms and Cr atoms at the interface is antiferromagnetic. The interlayer interaction is equivalent to a magnetic field as strong as B = 100.3 T applied by the NiO substrate to the $CrGeTe_3$ layer, which results in the higher Curie temperature of $CrGeTe_3$ observed in the experiment.

Keywords: 2D materials, first-principles calculation, $CrGeTe_3$/NiO interface, exchange interaction, heterostructure

OPEN ACCESS

Edited by:
Vincent G. Harris,
Northeastern University, United States

Reviewed by:
Xiaotian Wang,
Southwest University, China
Zhou Guanghui,
Hunan Normal University, China

****Correspondence:***
Xu Zuo
xzuo@nankai.edu.cn

Specialty section:
This article was submitted to Quantum Materials, a section of the journal Frontiers in Materials

Received: *02 March 2022*
Accepted: *02 May 2022*
Published: *08 June 2022*

Citation:
Liu X, Li Z, Zhang W, Yao P, Zhu H, Liu X and Zuo X (2022) First-Principles Calculations of the Exchange Interaction of the $CrGeTe_3$/NiO Interface. Front. Mater. 9:887864. doi: 10.3389/fmats.2022.887864

INTRODUCTION

Since the discovery of graphene (Novoselov et al., 2004; Geim and Novoselov, 2007; Geim, 2009), two-dimensional materials, such as hexagonal BN (Kubota et al., 2007) and transition metal dihalides (TMDs), have attracted considerable attention due to their novel properties and potential applications (Mak et al., 2010; Fang et al., 2012). Since a van der Waals heterostructure (Geim and Grigorieva, 2013) was proposed, the types of two-dimensional materials have been greatly enriched. The two-dimensional magnetic materials can be used in new spintronic devices with the advantages of high sensitivity and high storage density (Pesin and MacDonald, 2012; Han et al., 2014; Han, 2016). In the traditional isotropic Heisenberg model, any thermal fluctuation caused by finite temperature will destroy the long-range magnetic order in one- or two-dimensional systems, as stated in the so-called Mermin–Wagner theorem. However, recent studies have shown that magnetic anisotropy can bypass the Mermin–Wagner theorem and result in a long-range ferromagnetic order at finite temperature (Mermin and Wagner, 1966).

Both $CrGeTe_3$ and $CrSiTe_3$ monolayers are 2D ferromagnetic semiconductors, which makes them promising candidates for further applications in spintronics (Žutić et al., 2004; MacDonald et al., 2005; Geim and Grigorieva, 2013; Liu et al., 2016). The intrinsic ferromagnetism of $CrGeTe_3$ and $CrSiTe_3$ monolayers is due to the ferromagnetic superexchange interaction *via* the 90° Cr-Te-Cr path, which is mediated by the t_{2g} orbital exchange interaction of adjacent high-spin Cr^{3+} (Casto et al., 2015; Chen et al.,

2015; Williams et al., 2015; Liu et al., 2016; Gong et al., 2017). The bulk of $CrGeTe_3$ belongs to the van der Waals crystal, and the layers are bonded together along the c-axis by van der Waals force. This structure makes it easy to peel off a monolayer and combines it with other materials to form a heterostructure. By stacking two-dimensional material layers, the properties of materials can be improved and enhanced. For example, the Curie temperature of the $CrI_3/MoTe_2$ heterostructure is higher than that of CrI_3 alone (Chen et al., 2019). The Curie temperature of CrX_3 can be boosted by the heterostructure of CrX_3 and Mene (M = Si, Ge) (Li et al., 2019). Conversely, the band degeneracy at KK′ point of WSe_2 can be eliminated by using the neighbor exchange of CrI_3 (Zhong et al., 2017).

Recently, an experimental work found that $CrGeTe_3$ on the NiO substrate showed higher Curie temperature and stronger perpendicular magnetic anisotropy (Idzuchi et al., 2019). A $CrGeTe_3$/NiO heterojunction was prepared by depositing NiO on $CrGeTe_3$ flakes. Compared with the free-standing $CrGeTe_3$ flake, the hysteresis loop of the $CrGeTe_3$/NiO heterojunction became a square with a larger coercivity field (Idzuchi et al., 2019). When the thickness of NiO was 50 nm, the Curie temperature of $CrGeTe_3$/NiO heterojunction was as high as 115 K, while the maximum Curie temperature of $CrGeTe_3$ alone is only about 60K. In the experiment, $CrGeTe_3$ with a thickness of 5–200 nm was selected, and the Curie temperature of $CrGeTe_3$/NiO increased. Even if the thickness of the $CrGeTe_3$ flake reached 200 nm, the Curie temperature of $CrGeTe_3$/NiO was higher than that of bulk $CrGeTe_3$. It can be speculated that the antiferromagnet NiO is coupled with $CrGeTe_3$ through the proximity effect, which enhances the ferromagnetism of $CrGeTe_3$. However, the experiment neither gave further analysis nor clarified the micro mechanism of this phenomenon. Therefore, it is necessary to carry out theoretical calculation to explore the microcosmic mechanism behind the experimental phenomena.

In this study, we investigated the electronic structure and magnetism of the $CrGeTe_3$/NiO (111) interface atomistic model by the first-principles calculations and analyzed the interfacial exchange interaction of the $CrGeTe_3$/NiO (111) heterojunction.

APPROACH

The structure and electronic properties of the $CrGeTe_3$/NiO heterojunction are calculated by the density functional theory (DFT) and the projector-augmented wave (PAW) method implemented in the VASP code (Kresse and Furthmüller, 1996a; Kresse and Furthmüller, 1996b; Kresse and Joubert, 1999; Yu et al., 2009). The Perdew–Burke–Ernzerhof (PBE) parameterization of generalized gradient approximation (GGA) (Perdew et al., 1996) is applied as the exchange correlation functional. The on-site Coulomb interaction of 3d electrons in transition metalions strongly impacts the calculated electronic properties. In order to consider the strong localization effect of the d electrons in Cr and Ni atoms, the GGA + U method (Liechtenstein et al., 1995; Dudarev et al., 1998; Han and van Veenendaal, 2012) is applied to tune the spin properties of Cr and Ni atoms. The Hubbard U of Cr and Ni atoms are set to be 3.0 and 5.0 eV, respectively. In order to reduce the interference of the periodic interaction in the perpendicular direction, a vacuum region of 15 Å is added along the c-axis. The atomic positions are completely relaxed until the error of total energy and the residual force within 10^{-5} eV and 0.05 eV/Å, respectively. The energy cutoff of the plane wave basis is 520 eV. The Brillouin zone integral is performed on a Monkhorst–Pack k-mesh of $2 \times 2 \times 1$ size (Monkhorst and Pack, 1976). Along the high symmetry line Γ (0, 0, 0) → M (1/2, 0, 0) → K (1/3, 1/3, 0) → Γ (0, 0, 0), the band structure is calculated.

RESULTS AND DISCUSSION

According to the experimental results (Idzuchi et al., 2019), the thickness of $CrGeTe_3$ is 5.5–8 nm, while the thickness of NiO is 20–100 nm. Therefore, when building the model, the thickness of the NiO layer should be relatively large, while the thickness of the $CrGeTe_3$ layer is relatively small. In this work, four layers of NiO are used to simulate the substrate. For simplicity, a single layer of $CrGeTe_3$ is put on the NiO layers. In order to make the lattice match better, we selected the NiO (111) plane. In order to have stronger exchange at the interface, we set the Ni layer right at the interface. The optimized lattice constants of NiO (111) and $CrGeTe_3$ (001) surfaces are 5.895 Å and 6.913 Å, respectively. In the $CrGeTe_3$/NiO heterostructure model, $CrGeTe_3$ (001) ($\sqrt{3} \times \sqrt{3}$) is stacked on top of NiO (111) (2×2), and the lattice mismatch is about 1.6%. The thickness of the $CrGeTe_3$ (001) monolayer is 3.502 Å, where a unit cell includes 6 Cr, 6 Ge, and 18 Te atoms. The thickness of NiO (111) layers is 8.505 Å, where a unit cell includes 64 Ni and 64 O atoms. In addition, the lattice parameter of the heterojunction is a = b = 11.944 Å and c = 30.697 Å, and the initial interlayer distance (d) is 3.69 Å. The lower most Ni and O layers are fixed to simulate the NiO substrate, and other atoms are relaxed. **Figure 1A** shows the atomistic model of the $CrGeTe_3$/NiO heterojunction. In order to obtain the most stable magnetic ordering, two kinds of ferromagnetic (FM1 and FM2) and two kinds of antiferromagnetic (AFM1 and AFM2) orders of $CrGeTe_3$ are considered, as shown in **Figure 1B**. The magnetization direction of all Cr atoms in the FM1 order is upward, and the magnetization direction of all Cr atoms in the FM2 order is downward. The magnetization directions of the four Ni layers, from top to down, are ↑↓↑↓, and the magnetic order in the same layer of Ni atoms are ferromagnetic. This is the so-called "AFM II" magnetic order of bulk NiO. In the FM1 and FM2 orders, the magnetic coupling between $CrGeTe_3$ layer and NiO layer is ferromagnetic and antiferromagnetic, respectively.

The total energies of FM1, FM2, AFM1, and AFM2 are −744.05, −744.26, −743.97, and −744.14 eV, respectively. It is obvious that the total energy of FM2 state is the lowest. Its total magnetic moment is −18 μ_B. Therefore, the ground state of $CrGeTe_3$/NiO heterojunction is the FM2 state, where the exchange interaction in the $CrGeTe_3$ monolayer is ferromagnetic and that between the $CrGeTe_3$ monolayer and the NiO layers is antiferromagnetic. In order to investigate the stability of the FM2 interface system, we further calculated the binding energy, which is defined as

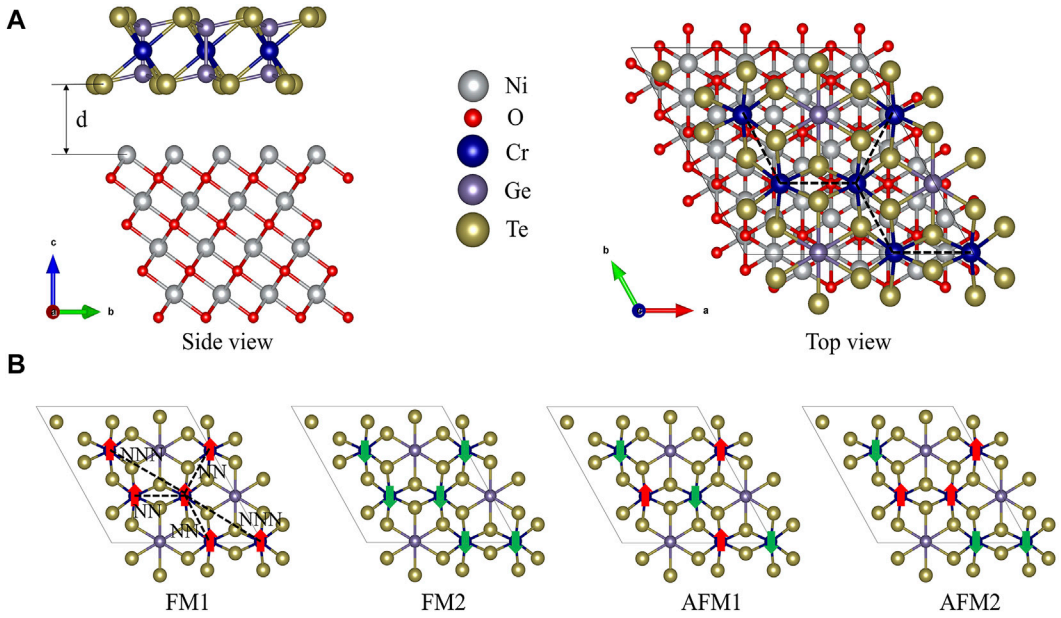

FIGURE 1 | (A) Top and side views of the $CrGeTe_3$/NiO heterostructure. **(B)** Four possible magnetic states of $CrGeTe_3$: FM1, FM2, AFM1, and AFM2.

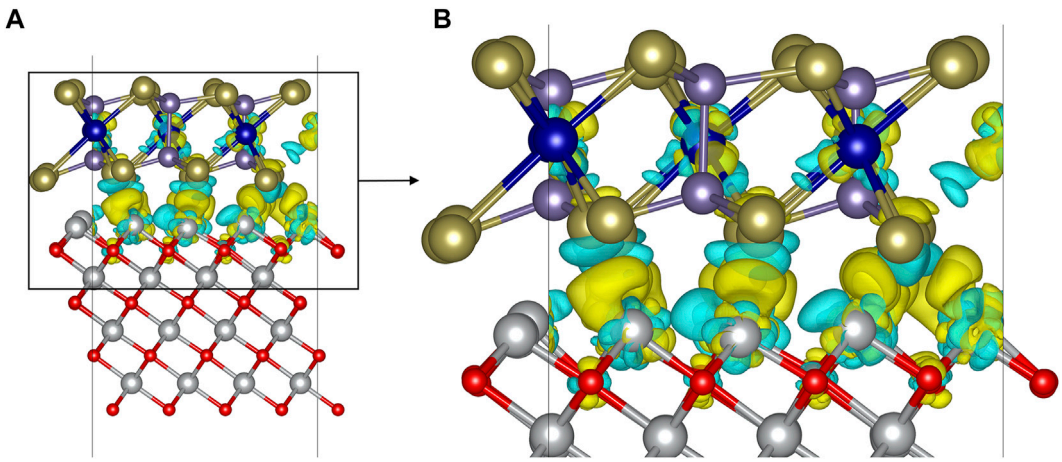

FIGURE 2 | Differential charge density **(A)** and its local enlarged view **(B)** of the $CrGeTe_3$/NiO interface in the FM2 state. The isosurface is set to 0.021 e/Å^3.

$E_f = E_{tot} - E_{CrGeTe_3} - E_{NiO}$. Here, E_{tot} is the total energy of the heterostructure, E_{CrGeTe_3} (E_{NiO}) is the total energy of the isolated $CrGeTe_3$ (NiO). The binding energy of the FM2 state is −0.067 eV/Å^2. The negative binding energy of the FM2 state shows that the heterostructure is energetically preferred and can be realized in the experiment. We calculated the phonon spectra (Xie et al., 2021) of NiO (111) and $CrGeTe_3$ (001) surfaces in the FM2 state. The results showed that there is no virtual frequency, which means that the structures of NiO (111) and $CrGeTe_3$ (001) surfaces are stable.

In order to obtain the detailed charge transfer information of the interface, the charge density difference and Bader charge of the $CrGeTe_3$/NiO heterojunction in the FM2 state are calculated. Charge density difference is the redistribution of charge as the $CrGeTe_3$ monolayer is bound to the NiO substrate. In the interface calculation, the bonding of each atom at the interface can be intuitively shown by the charge density difference. The charge density difference can be expressed as $\Delta\rho = \rho_{CrGeTe_3/NiO} - \rho_{CrGeTe_3} - \rho_{NiO}$. Among them, $\Delta\rho$ is the difference of charge density, $\rho_{CrGeTe_3/NiO}$ is the total charge density of the heterojunction system, and ρ_{CrGeTe_3} (ρ_{NiO}) is the charge density of $CrGeTe_3$ (NiO) slab alone.

Figure 2A shows the charge density difference of the $CrGeTe_3$/NiO interface in the FM2 state, and **Figure 2B** zooms in the details of **Figure 2A**. The cyan area in **Figure 2** indicates that the charge density difference is negative, and the yellow region indicates the charge density difference is positive. In **Figure 2**, the charge transfer

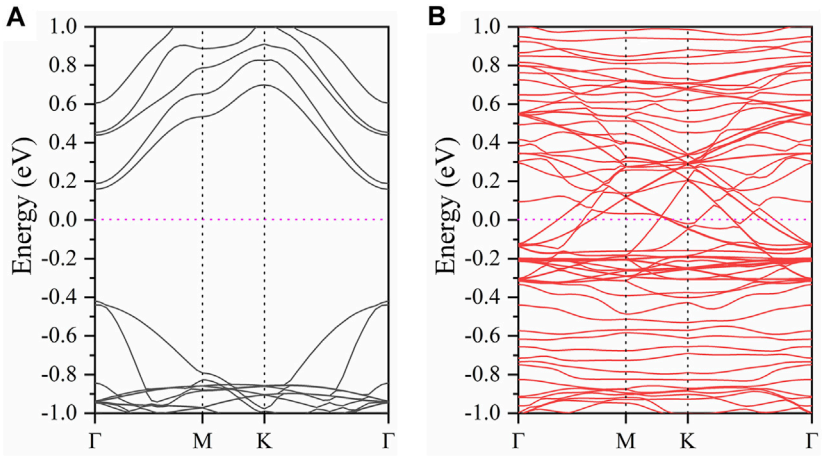

FIGURE 3 | Band structure of the $CrGeTe_3$/NiO heterojunction in the FM2 state. **(A)** and **(B)** represent the spin-up and spin-down channels, respectively. The Fermi level is set to zero.

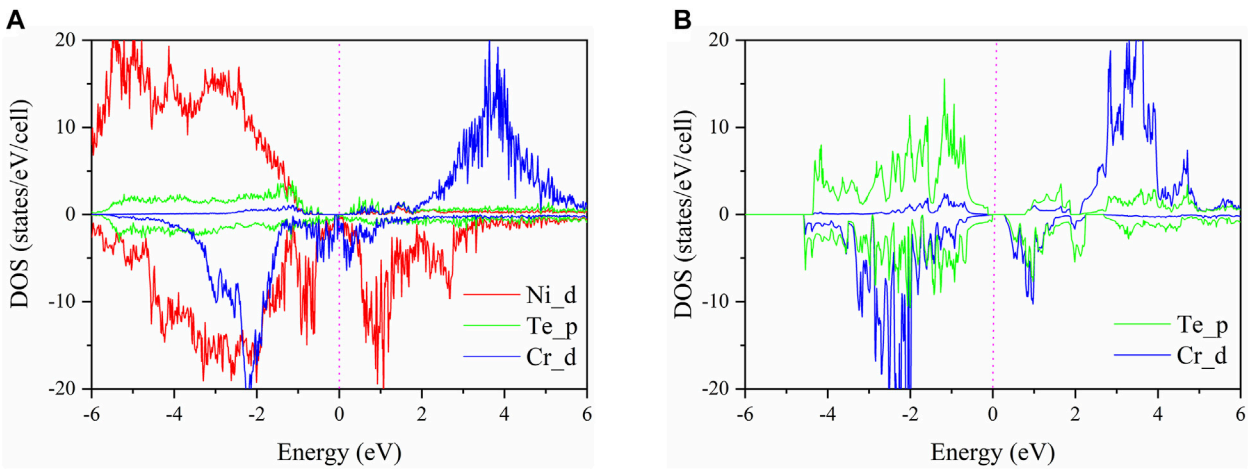

FIGURE 4 | (A) Projected density of states (PDOS) for the $CrGeTe_3$/NiO interface in the FM2 state. **(B)** Projected density of states (PDOS) for $CrGeTe_3$ alone. The Fermi level is set to zero.

results in Ni and Te weak covalent bonds across the interface. In order to further analyze the mechanism of charge transfer, Bader charge analysis is carried out for the system. The results showed that about 1.166 electron is transferred from NiO to $CrGeTe_3$. The charge transfer mainly occurs between the Ni, Te, and Cr atoms near the interface. In the binding process, a Te atom near the interface gets 0.098 electron in average, a Cr atom gets 0.060 electron in average, and the charge change of each Ge atom is negligible. However, the charge redistribution of the atoms away from the interface is negligible as they do not participate in the binding process.

In order to study the electronic properties of the $CrGeTe_3$/NiO interface in the FM2 state, the band structure and density of states of the model are calculated. The band structure of the $CrGeTe_3$/NiO heterojunction in the FM2 state is shown in **Figure 3**. The spin-up and spin-down band gaps are 0.578 and 0 eV, respectively. The total band gap is 0 eV. As a comparison, the band gaps of NiO and $CrGeTe_3$ bulk are calculated to be 2.026 and 0.236 eV, respectively, and those of the NiO (111) surface and $CrGeTe_3$ (001) monolayer are 0.003 and 0.256 eV, respectively. It is obvious that the band gap of the NiO (111) surface is much smaller than that of NiO bulk, and the band gap of the $CrGeTe_3$ (001) monolayer is very close to that of $CrGeTe_3$ bulk. The band gap of the $CrGeTe_3$/NiO heterojunction in the FM2 state is 0 eV, which is smaller than the NiO (111) surface band gap and $CrGeTe_3$ (001) monolayer.

The projected density of states of Ni, Te, and Cr atoms near the interface of the $CrGeTe_3$/NiO heterojunction in the FM2 state is shown in **Figure 4A**. The projected density of states of Te and Cr atoms of the $CrGeTe_3$ alone is shown in **Figure 4B**. From **Figure 4A**, it is clear that the state near Fermi level is mainly

contributed by the orbitals of Ni, Te, and Cr atoms. Among them, the contribution of the Cr-3d orbital is the largest. The Cr 3d state, the Ni 3d state, and the Te 5p state all pass through the Fermi level. From **Figure 4B**, it is clear that the state near Fermi level is mainly contributed by the orbitals of Te and Cr atoms. The band gap of $CrGeTe_3$ alone is 0.236 eV, which is significantly larger than that of $CrGeTe_3$/NiO heterojunction.

By comparing the PDOS in **Figures 4A,B**, for the spin-up state, it is seen that some new electronic states appear on the $CrGeTe_3$/NiO interface from 0.104 to 0.774 eV nearby the Fermi level. Some electronic states disappear from −0.394 to −0.114 eV nearby the Fermi level. These new electronic states lead to the downward movement of the top of the valence band and the bottom of the conduction band. The final result is that the band gap of the spin-up state of the $CrGeTe_3$/NiO heterojunction becomes smaller. For the spin-down state, it is seen that some new electronic states appear on the $CrGeTe_3$/NiO interface from −0.002 to 0.236 eV nearby the Fermi level. The appearance of these new electronic states leads to the upward movement of the top of the valence band and the downward movement of the bottom of the conduction band. The end result is that the band gap of the spin-down state of the $CrGeTe_3$/NiO heterojunction is reduced to zero.

The occupied Cr-3d orbital cannot appear in both spin-up and spin-down directions. For example, when it is found in the spin-down direction, the spin-up Cr-3d orbital is completely unoccupied. These results can be understood by crystal field theory. Cr^{3+} ions are located in an octahedral environment coordinated by six Te anions. The Cr-3d orbital splits into three low energy t_{2g} orbitals and two high energy e_g orbitals. According to Pauli's exclusion principle and Hund's rule, Cr^{3+} ions will present a high-spin $t_{2g}^{3}e_g^{0}$ electronic configuration, which means that all occupied 3d orbits must be in one spin direction. Among them, the Cr 3d state also contributes to the spin-down state. Also, higher than the Fermi level, the spin-up state is almost occupied by the Cr 3d state, and the spin-down state is almost occupied by the Ni 3d state.

In order to estimate the magnetic couplings in the $CrGeTe_3$/NiO heterojunction, we started from the Heisenberg model:

$$H = -\sum_{i<j} J_{ij}\boldsymbol{S}_i \cdot \boldsymbol{S}_j, \tag{1}$$

and it can be rewritten for our specific model:

$$H = -\sum_{i<j} J_1\boldsymbol{S}_i \cdot \boldsymbol{S}_j - \sum_{k<l} J_2\boldsymbol{S}_k \cdot \boldsymbol{S}_l - \sum_{m<n} J_0\boldsymbol{S}_m \cdot \boldsymbol{S}_n, \tag{2}$$

where J_1 is the intralayer exchange interaction between a Cr atom and its nearest-neighbors (NN), J_2 is the intralayer exchange interaction between a Cr atom and its next-nearest-neighbors (NNN), and J_0 is the interlayer exchange interaction parameter between a Cr atom and its NN Ni atoms in the top layer of NiO. The Ni atoms in the lower three layers of NiO are not considered in this model because of their weak exchange interaction with the Cr atoms. S_i-S_m is the spin of a Cr atom (S) equal to 3/2. S_n is the spin of a Ni atom (S_{Ni}) equal to 1.

In the $CrGeTe_3$ layer, there are three NN and six NNN Cr atoms for a Cr atom. In FM1 and FM2 structures, there are three NN spin parallel Cr atoms and six NNN spin parallel Cr atoms for a Cr atom. For the interlayer exchange interaction with the NiO substrate, the exchange interaction between a Cr atom and three nearest neighbor Ni atoms is considered. Because the spin directions of Cr and Ni atoms are the same, the interlayer coupling in the FM1 structure is ferromagnetic. Because the spin direction of Cr atom and Ni atom is opposite, the interlayer coupling in the FM2 structure is antiferromagnetic. For an AFM1 structure, there are three NN antiparallel spin Cr atoms and six NNN parallel spin Cr atoms for each Cr atom. In addition, because the sum of the spin of Cr atoms is zero, the summation of the exchange interaction between Cr and Ni atoms is also zero. For the AFM2 structure, the situation is complicated. The interlayer magnetic coupling is the same as AFM1, which is zero. For intralayer magnetic coupling, there are four Cr atoms with one NN parallel spin and two NN antiparallel spin Cr atoms. At the same time, these four Cr atoms also have three NNN parallel spin and three NNN antiparallel spin Cr atoms. The other two Cr atoms have two NN parallel spin and one NN antiparallel spin Cr atoms. At the same time, these two Cr atoms also have six NNN antiparallel spin Cr atoms. Therefore, the total energies of the $CrGeTe_3$/NiO heterojunction in four magnetic states can be written as follows:

$$\begin{cases} E_{FM1} = E_0 - 9J_1|\boldsymbol{S}|^2 - 18J_2|\boldsymbol{S}|^2 - 18J_0|\boldsymbol{S}\cdot\boldsymbol{S}_{Ni}|, \\ E_{FM2} = E_0 - 9J_1|\boldsymbol{S}|^2 - 18J_2|\boldsymbol{S}|^2 + 18J_0|\boldsymbol{S}\cdot\boldsymbol{S}_{Ni}|, \\ E_{AFM1} = E_0 + 9J_1|\boldsymbol{S}|^2 - 18J_2|\boldsymbol{S}|^2, \\ E_{AFM2} = E_0 + J_1|\boldsymbol{S}|^2 + 6J_2|\boldsymbol{S}|^2, \end{cases} \tag{3}$$

where E_0 is the total energy excluding the magnetic coupling that is insensitive to the magnetic states. By eliminating E_0, the exchange constants are solved as follows:

$$\begin{cases} J_0 = \dfrac{E_{FM2} - E_{FM1}}{36|\boldsymbol{S}\cdot\boldsymbol{S}_{Ni}|}, \\ J_1 = \dfrac{E_{AFM1} - \dfrac{E_{FM1} + E_{FM2}}{2}}{18|\boldsymbol{S}|^2}, \\ J_2 = \dfrac{J_1}{3} - \dfrac{E_{AFM1} - E_{AFM2}}{24|\boldsymbol{S}|^2}. \end{cases} \tag{4}$$

Substituting the calculated total energies of the four magnetic states into **Eq. 4**, we can get the following exchange interaction parameters: $J_0 = -3.87\,meV$, $J_1 = +4.76\,meV$, and $J_2 = -1.73\,meV$. It is clear that the intralayer exchange interaction between the NN Cr atoms is ferromagnetic, which is consistent with the previous experimental result that the $CrGeTe_3$ monolayer is a two-dimensional intrinsic ferromagnet (Gong et al., 2017). In addition, the interlayer exchange interaction between the Ni and Cr atoms is antiferromagnetic. An intralayer ferromagnetic interaction between the nearest Cr atoms is produced close to the 90° Cr-Te-Cr superexchange channel. At the same time, the interlayer antiferromagnetic interaction between Cr and Ni atoms is produced by approaching the 120° Cr-Te-Ni superexchange channel.

Magnets with large magnetic anisotropy energy (MAE) have potential applications in magnetic storage. Magnetic anisotropy can avoid the Mermin–Wagner theorem and make a detour to long-

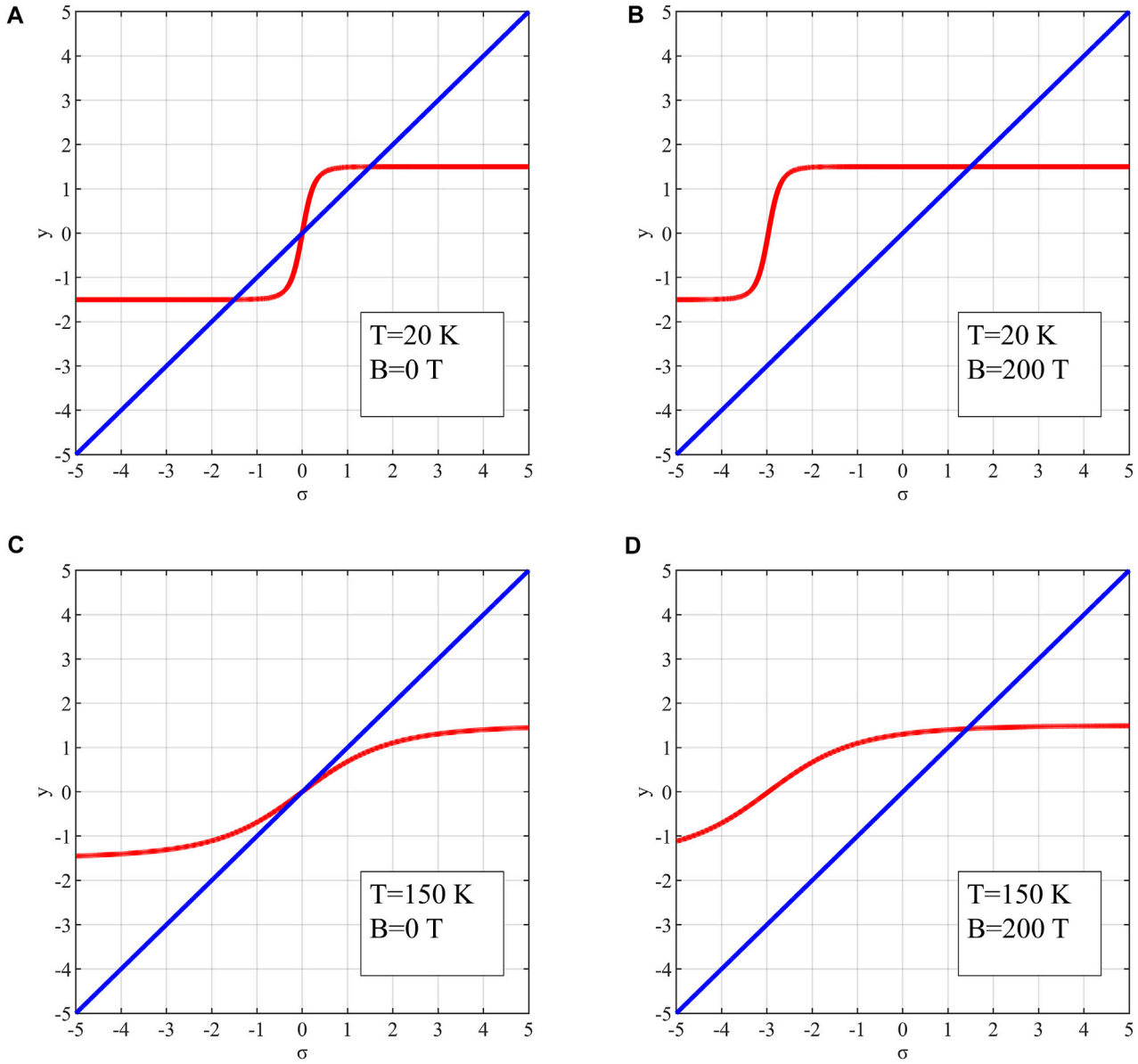

FIGURE 5 | Two functions in **Eq. 10** with different parameter sets: **(A)** $T = 20\,K$, $B = 0\,T$; **(B)** $T = 20\,K$, $B = 200\,T$; **(C)** $T = 150\,K$, $B = 0\,T$; **(D)** $T = 150\,K$, $B = 200\,T$. The red line represents $y = SB_S\left(\frac{2S_iJ(0)}{k_BT}\sigma + \frac{g\mu_BSB}{k_BT}\right)$, and the blue line represents $y = \sigma$.

range magnetic order in two-dimensional magnets at a non-zero temperature (Mermin and Wagner, 1966; Torelli et al., 2019). MAE is defined as the energy difference when magnetization is in-plane and out-of-plane, respectively ($MAE = E_{\parallel} - E_{\perp}$), where $E_{\parallel}$ is the total energy with the in-plane magnetization direction, and $E_{\perp}$ is that with out-of-plane magnetization direction. The positive (negative) value of MAE represents that the out-of-plane (in-plane) is energetically preferred. The MAE of the $CrGeTe_3$/NiO heterojunction is calculated by enabling spin-orbit coupling (SOC). The easy axis is in-plane with a MAE of −0.094 meV/Å^2.

The previous experimental result indicates that the $CrGeTe_3$/NiO heterostructure shows a higher Curie temperature than the free-standing $CrGeTe_3$ monolayer (Idzuchi et al., 2019). Therefore, we showed that the Ni–Cr interlayer exchange leads to the increase in Curie temperature of $CrGeTe_3$.

The total exchange energy (Zhong et al., 2017) between the Cr and Ni atoms is $\Delta E = \frac{E_{FM1} - E_{FM2}}{2} = 104.54\,meV$ by the *ab initio* calculations. Because there are six Cr atoms in the cell, the average exchange energy of each Cr atom is $\bar{E} = 17.42\,meV$.

In the Zeeman effect, it is written as follows:

$$\bar{E} = -g\mu_B \boldsymbol{S} \cdot \boldsymbol{B}, \tag{5}$$

where g is the g factor ($g \approx 2$), μ_B is the Bohr magneton, S is the spin of Cr^{3+} ion ($S = 3/2$), and B is the magnetic induction intensity. Substituting the *ab initio* value into **Eq. 5**, we obtained $B = 100.3$ T,

which is the equivalent magnetic field exerted by the NiO substrate on to the $CrGeTe_3$ layer. The influence of the NiO substrate on the Curie temperature of the $CrGeTe_3$ monolayer by the interlayer magnetic coupling is analyzed by means of mean field theory.

Brillouin function is defined by Yosida (1996) as follows:

$$B_S(x) = \frac{2S+1}{2S}\coth\left(\frac{2S+1}{2S}x\right) - \frac{1}{2S}\coth\left(\frac{1}{2S}x\right), \quad (6)$$

where S is the spin of Cr atom, and the value of x is as follows:

$$x = \frac{2S\sigma\mathcal{J}(0) + g\mu_B SB}{k_B T}, \quad (7)$$

where σ is the thermo average magnetic moment of Cr atom, k_B is Boltzmann's constant, T is temperature, and $J(0)$ is defined by

$$\mathcal{J}(\boldsymbol{q}) = \sum_n J(\boldsymbol{R_n})e^{-i\boldsymbol{q}\cdot\boldsymbol{R_n}}, \quad (8)$$

where $J(R_n)$ is the exchange interaction between the lattice sites, and q is the vector in the reciprocal space. Substituting the exchange constant obtained before, the value of $\mathcal{J}(0)$ is approximately calculated as follows:

$\mathcal{J}(0) = \sum_n J(\mathrm{R}_n) = 3J_1 + 6J_2 = 3.90\,meV = 6.25 \times 10^{-22}\,J$.

At thermo equilibrium, the following equation can be obtained as follows:

$$\sigma = SB_S\left(\frac{2S\mathcal{J}(0)}{k_B T}\sigma + \frac{g\mu_B SB}{k_B T}\right). \quad (9)$$

The left and right sides of **Eq. 9** are two functions, respectively, as follows:

$$\begin{cases} y = \sigma, \\ y = SB_S\left(\dfrac{2S\mathcal{J}(0)}{k_B T}\sigma + \dfrac{g\mu_B SB}{k_B T}\right). \end{cases} \quad (10)$$

At fixed temperature T and magnetic induction intensity B, the solutions of **Eq. 9** are the intersection points of the two curves of **Eq. 10**, as shown in **Figure 5**.

In **Figures 5A,C**, there is no equivalent external field, while there is in **Figures 5B,D**. In **Figure 5A**, two functions crossover in the first quadrant, indicating that **Eq. 9** has a non-zero solution of σ, which is the average magnetic moment of Cr atom below Curie temperature. In **Figure 5C**, there is only one intersection point at the origin, which indicates that the spontaneous magnetization vanishes when the temperature is above the Curie temperature. However, when the external field is not zero, as shown in **Figures 5B,D**, even if the temperature is higher than the Curie temperature at zero extra field, there is still a non-zero solution of σ, which implies the rise of Curie temperature.

By taking different T values under $B = 0\,T$, $10\,T$, $100\,T$, and $200\,T$ and solving **Eq. 9**, the $\sigma - T$ figure is platted in **Figure 6**:

It is noticeable that the decrease of σ with the increase of T is much slower at $B = 100\,T$ than at $B = 0\,T$. It indicates that the heterostructure of $CrGeTe_3$ and NiO is equivalent to applying a strong magnetic field on the $CrGeTe_3$ monolayer. Thus, the Curie temperature is boosted.

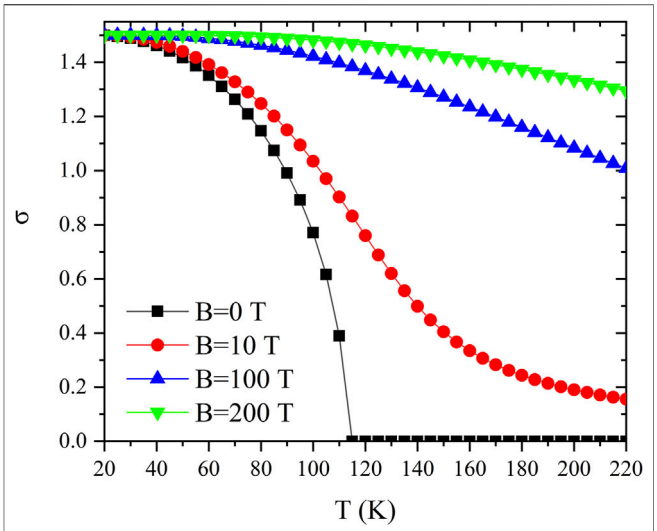

FIGURE 6 | $\sigma - T$ curves at different values of B.

CONCLUSION

In summary, we built the $CrGeTe_3$/NiO heterojunction model and discovered that the interlayer exchange interaction between the Cr atoms and Ni atoms is antiferromagnetic using the first-principles calculations. We further calculated the electrical and magnetic properties of the $CrGeTe_3$/NiO interface. We inferred that the NiO substrate is equivalent to applying a strong magnetic field of $B = 100.3$ T on the $CrGeTe_3$ layer, which is the reason for the increase of Curie temperature. In addition, the easy axis is in-plane with a MAE of −0.094 meV/Å^2.

DATA AVAILABILITY STATEMENT

The raw data supporting the conclusion of this article will be made available by the authors, without undue reservation.

AUTHOR CONTRIBUTIONS

XuL and XZ conceived and implemented the review process. XuL was responsible for the main writing of the manuscript. XZ was responsible for the modification of the manuscript. ZL helped process and check the data part. WZ and HZ helped to build the structure model and provide ideas on magnetic calculation. PY and XiL provided ideas on electronic structure calculation. All authors contributed to the manuscript and approved the submitted version.

FUNDING

This research is supported by the Science Challenge Project (Grant No. TZ2016003-1-105), the Tianjin Natural Science Foundation (Grant No. 20JCZDJC00750), and the Fundamental Research Funds for the Central Universities-Nankai University (Grant No 63211107 and 63201182).

REFERENCES

Casto, L. D., Clune, A. J., Yokosuk, M. O., Musfeldt, J. L., Williams, T. J., Zhuang, H. L., et al. (2015). Strong Spin-Lattice Coupling in CrSiTe3. *Apl. Mater.* 3, 041515. doi:10.1063/1.4914134

Chen, S., Huang, C., Sun, H., Ding, J., Jena, P., and Kan, E. (2019). Boosting the Curie Temperature of Two-Dimensional Semiconducting CrI3 Monolayer through van der Waals Heterostructures. *J. Phys. Chem. C* 123, 17987–17993. doi:10.1021/acs.jpcc.9b04631

Chen, X., Qi, J., and Shi, D. (2015). Strain-engineering of Magnetic Coupling in Two-Dimensional Magnetic Semiconductor CrSiTe3: Competition of Direct Exchange Interaction and Superexchange Interaction. *Phys. Lett. A* 379, 60–63. doi:10.1016/j.physleta.2014.10.042

Dudarev, S. L., Botton, G. A., Savrasov, S. Y., Humphreys, C. J., and Sutton, A. P. (1998). Electron-Energy-Loss Spectra and the Structural Stability of Nickel Oxide: An LSDA+U Study. *Phys. Rev. B* 57, 1505–1509. doi:10.1103/PhysRevB.57.1505

Fang, H., Chuang, S., Chang, T. C., Takei, K., Takahashi, T., and Javey, A. (2012). High-Performance Single Layered WSe2 P-FETs with Chemically Doped Contacts. *Nano Lett.* 12, 3788–3792. doi:10.1021/nl301702r

Geim, A. K. (2009). Graphene: Status and Prospects. *Science* 324, 1530–1534. doi:10.1126/science.1158877

Geim, A. K., and Grigorieva, I. V. (2013). Van der Waals heterostructures. *Nature* 499, 419–425. doi:10.1038/nature12385

Geim, A. K., and Novoselov, K. S. (2007). The Rise of Graphene. *Nat. Mater* 6, 183–191. doi:10.1038/nmat1849

Gong, C., Li, L., Li, Z., Ji, H., Stern, A., Xia, Y., et al. (2017). Discovery of intrinsic ferromagnetism in two-dimensional van der Waals crystals. *Nature* 546, 265–269. doi:10.1038/nature22060

Han, M. J., and van Veenendaal, M. (2012). Spin-moment Formation and Reduced Orbital Polarization in LaNiO3/LaAlO3superlattice:LDA+Ustudy. *Phys. Rev. B* 85, 195102. doi:10.1103/PhysRevB.85.195102

Han, W., Kawakami, R. K., Gmitra, M., and Fabian, J. (2014). Graphene Spintronics. *Nat. Nanotech* 9, 794–807. doi:10.1038/nnano.2014.214

Han, W. (2016). Perspectives for Spintronics in 2D Materials. *Apl. Mater.* 4, 032401. doi:10.1063/1.4941712

Idzuchi, H., Llacsahuanga Allcca, A. E., Pan, X. C., Tanigaki, K., and Chen, Y. P. (2019). Increased Curie Temperature and Enhanced Perpendicular Magneto Anisotropy of Cr2Ge2Te6/NiO Heterostructures. *Appl. Phys. Lett.* 115, 232403. doi:10.1063/1.5130930

Kresse, G., and Furthmüller, J. (1996). Efficiency of Ab-Initio Total Energy Calculations for Metals and Semiconductors Using a Plane-Wave Basis Set. *Comput. Mater. Sci.* 6, 15–50. doi:10.1016/0927-0256(96)00008-0

Kresse, G., and Furthmüller, J. (1996). Efficient Iterative Schemes Forab Initiototal-Energy Calculations Using a Plane-Wave Basis Set. *Phys. Rev. B* 54, 11169–11186. doi:10.1103/PhysRevB.54.11169

Kresse, G., and Joubert, D. (1999). From Ultrasoft Pseudopotentials to the Projector Augmented-Wave Method. *Phys. Rev. B* 59, 1758–1775. doi:10.1103/PhysRevB.59.1758

Kubota, Y., Watanabe, K., Tsuda, O., and Taniguchi, T. (2007). Deep Ultraviolet Light-Emitting Hexagonal Boron Nitride Synthesized at Atmospheric Pressure. *Science* 317, 932–934. doi:10.1126/science.1144216

Li, H., Xu, Y.-K., Lai, K., and Zhang, W.-B. (2019). The enhanced ferromagnetism of single-layer CrX3 (X = Br and I) via van der Waals engineering. *Phys. Chem. Chem. Phys.* 21, 11949–11955. doi:10.1039/C9CP01837A

Liechtenstein, A. I., Anisimov, V. I., and Zaanen, J. (1995). Density-functional Theory and Strong Interactions: Orbital Ordering in Mott-Hubbard Insulators. *Phys. Rev. B* 52, R5467–R5470. doi:10.1103/PhysRevB.52.R5467

Liu, B., Zou, Y., Zhang, L., Zhou, S., Wang, Z., Wang, W., et al. (2016). Critical Behavior of the Quasi-Two-Dimensional Semiconducting Ferromagnet CrSiTe3. *Sci. Rep.* 6, 33873. doi:10.1038/srep33873

MacDonald, A. H., Schiffer, P., and Samarth, N. (2005). Ferromagnetic Semiconductors: Moving beyond (Ga,Mn)As. *Nat. Mater* 4, 195–202. doi:10.1038/nmat1325

Mak, K. F., Lee, C., Hone, J., Shan, J., and Heinz, T. F. (2010). Atomically ThinMoS2: A New Direct-Gap Semiconductor. *Phys. Rev. Lett.* 105, 136805. doi:10.1103/PhysRevLett.105.136805

Mermin, N. D., and Wagner, H. (1966). Absence of Ferromagnetism or Antiferromagnetism in One- or Two-Dimensional Isotropic Heisenberg Models. *Phys. Rev. Lett.* 17, 1133–1136. doi:10.1103/physrevlett.17.1133

Monkhorst, H. J., and Pack, J. D. (1976). Special Points for Brillouin-Zone Integrations. *Phys. Rev. B* 13, 5188–5192. doi:10.1103/physrevb.13.5188

Novoselov, K. S., Geim, A. K., Morozov, S. V., Jiang, D., Zhang, Y., Dubonos, S. V., et al. (2004). Electric Field Effect in Atomically Thin Carbon Films. *Science* 306, 666–669. doi:10.1126/science.1102896

Perdew, J. P., Burke, K., and Ernzerhof, M. (1996). Generalized Gradient Approximation Made Simple. *Phys. Rev. Lett.* 77, 3865–3868. doi:10.1103/physrevlett.77.3865

Pesin, D., and MacDonald, A. H. (2012). Spintronics and Pseudospintronics in Graphene and Topological Insulators. *Nat. Mater* 11, 409–416. doi:10.1038/nmat3305

Torelli, D., Thygesen, K. S., and Olsen, T. (2019). High Throughput Computational Screening for 2D Ferromagnetic Materials: the Critical Role of Anisotropy and Local Correlations. *2D Mat.* 6, 045018. doi:10.1088/2053-1583/ab2c43

Williams, T. J., Aczel, A. A., Lumsden, M. D., Nagler, S. E., Stone, M. B., Yan, J.-Q., et al. (2015). Magnetic Correlations in the Quasi-Two-Dimensional Semiconducting ferromagnetCrSiTe3. *Phys. Rev. B* 92, 144404. doi:10.1103/physrevb.92.144404

Xie, C., Liu, Y., Zhang, Z., Zhou, F., Yang, T., Kuang, M., et al. (2021). Sixfold Degenerate Nodal-point Phonons: Symmetry Analysis and Materials Realization. *Phys. Rev. B* 104, 045148. doi:10.1103/PhysRevB.104.045148

Yosida, K. (1996). *Theory of Magnetism*. Berlin: Springer.

Yu, J., Lin, X., Wang, J., Chen, J., and Huang, W. (2009). First-principles Study of the Relaxation and Energy of Bcc-Fe, Fcc-Fe and AISI-304 Stainless Steel Surfaces. *Appl. Surf. Sci.* 255, 9032–9039. doi:10.1016/j.apsusc.2009.06.087

Zhong, D., Seyler, K. L., Linpeng, X., Cheng, R., Sivadas, N., Huang, B., et al. (2017). Van der Waals engineering of ferromagnetic semiconductor heterostructures for spin and valleytronics. *Sci. Adv.* 3, e1603113. doi:10.1126/sciadv.1603113

Žutić, I., Fabian, J., and Das Sarma, S. (2004). Spintronics: Fundamentals and Applications. *Rev. Mod. Phys.* 76, 323–410. doi:10.1103/RevModPhys.76.323

Conflict of Interest: The authors declare that the research was conducted in the absence of any commercial or financial relationships that could be construed as a potential conflict of interest.

Publisher's Note: All claims expressed in this article are solely those of the authors and do not necessarily represent those of their affiliated organizations, or those of the publisher, the editors, and the reviewers. Any product that may be evaluated in this article, or claim that may be made by its manufacturer, is not guaranteed or endorsed by the publisher.